



# SFERA-III

Solar Facilities for the European Research Area

## Algorithms for intrahour DNI forecasting

Deliverable D10.2 (D37)

Estimated delivery date: 31.12.2022

Actual delivery date: 24.01.2023

Lead beneficiary: CNRS

Person responsible: Stéphane Thil

Deliverable type:  R  DEM  DEC  OTHER  ETHICS  ORDP

Dissemination level:  PU  CO  EU-RES  EU-CON  EU-SEC



## AUTHORS

Author	Institution	E-mail
S. Thil	PROMES-CNRS	stephane.thil@univ-perp.fr

## DOCUMENT HISTORY

Version	Date	Change
1.0	01/2023	

## VALIDATION

Reviewers	Validation date
M. Röger	DLR (WP 10 lead)
	10.02.23

## DISTRIBUTION LIST

Date	Recipients

## Disclaimer

The content of this publication reflects only the author's view and not necessary those of the European Commission. Furthermore, the Commission is not responsible for any use that may be made of the information this publication contains.

# Executive Summary

This report summarizes the work done in Subtask 10.2.1, that aims at increasing the useful on-Sun experimental time available to RI users during their stay, by providing accurate intrahour forecasts of direct normal irradiance (DNI).

A hybrid intrahour forecast model has been developed, combining knowledge-based and machine-learning approaches and taking DNI measurements and HDR sky images as inputs. The results show that this algorithm is capable of outperforming the smart persistence model, as well as machine-learning-based models using past DNI observations only, for various forecast horizons.

The work has lead to several scientific publications listed below.

- [PhD thesis] Y. Karout. Pr evision de l' claircissement normal direct par intelligence artificielle et commande pr dictive d'un r acteur solaire. PhD thesis, Universit  de Perpignan Via Domitia, Dec. 2022.
- [Conference 1] Y. Karout, S. Thil, J. Eynard, and S. Grieu. Cloud/sky segmentation from ground camera based on supervised machine learning approach. In 33rd International Conference on Efficiency, Cost, Optimization, Simulation and Environmental Impact of Energy Systems (ECOS 2020), Osaka, Japan, July 2020.
- [Conference 2] Y. Karout, A. Curcio, J. Eynard, S. Thil, S. Rodat, S. Abanades, and S. Grieu. Model-based predictive control of a solar reactor dedicated to syngas production. In 28th International Conference on Concentrating Solar Power and Chemical Energy Systems (SolarPACES 2022), 2022.
- [Conference 3] Y. Karout, S. Thil, J. Eynard, E. Guillot, and S. Grieu. Intrahour direct normal irradiance forecasting based on sky image processing and time-series analysis. In 28th International Conference on Concentrating Solar Power and Chemical Energy Systems (SolarPACES 2022), 2022.
- [Article 1] Y. Karout, S. Thil, J. Eynard, E. Guillot, and S. Grieu. Hybrid intrahour DNI forecast model based on DNI measurements and sky-imaging data. *Solar Energy*, 249:541–558, Jan. 2023.

## Table of Contents

---

Executive Summary .....	3
Table of Contents .....	4
1. Introduction .....	5
2. DNI and sky images database .....	6
3. Reference forecasting models .....	8
3.1. Persistence model .....	8
3.2. Smart persistence model.....	8
3.3. Machine-learning-based models.....	9
3.3.1. LSTM model .....	9
3.3.2. CNN-LSTM model.....	10
3.3.3. Implementation of machine-learning-based models.....	11
3.4. Proposed hybrid forecasting model.....	12
3.4.1. Image processing.....	12
3.4.2. DNI forecast model.....	13
3.5. Forecasting results.....	14
3.5.1. Performance metrics .....	14
3.5.2. Comparison of forecasting results .....	15
3.6. Online implementation of the hybrid model.....	20
3.7. Conclusion.....	22
List of abbreviations.....	23
Annexes .....	24
Annex 1. References.....	25
Annex 2. Scientific article published in “Solar Energy” .....	25
Annex 3. Complete PhD thesis .....	25

# 1. Introduction

The main approaches to forecast direct normal irradiance (DNI) are statistical models, image-based models, and numerical weather prediction (NWP) models. Each approach is characterized by a range of spatio-temporal horizons. Statistical models can provide forecasts with high temporal resolutions and for long forecast horizons, but they are limited by low spatial capabilities. On the other hand, the NWP models, that solve weather equations to forecast irradiance, are characterized by very high spatio-temporal capability and are capable of handling high forecast horizons, but are highly dependent on the initial state of the variables used in the equations (which in turn requires accurate measurements with specific sensors that must be distributed wisely) and demand important computational resources for low forecast resolutions. Finally, image-based models provide high spatio-temporal resolution with less computational requirements compared to the NWP models (the complexity of image-based models depends on the code optimization and the type of algorithms implemented in the image processing steps).

As this task is interested in intrahour DNI forecasting, the focus is on statistical and ground-based sky imagery models.

A hybrid forecast model is proposed, that can harness the advantages of both approaches. This model is compared to the smart persistence model and two machine-learning-based models using only past DNI observations as input.

## 2. DNI and sky images database

The first action in this task was to select a sky imager delivering high-quality images. The chosen sky imager provides HDR images with a 1300x1216 effective resolution and was installed at the Odeillo solar furnace (Figure 1).



Figure 1. **Sky imager at Odeillo solar furnace.**

A database of HDR sky images (collected each 30 seconds, using the sky imager above) and DNI measurements (collected each second, using a PROMES-CNRS pyrhelimeter) has then been constituted. The quality of the data is crucial, since machine learning methods are used to forecast DNI. Compared to the usually-used low dynamic range images, HDR images have the distinct advantage of being less saturated in the circumsolar area, thus providing additional and important information. This is especially important for short forecast horizons, since we then need to examine parts of the image closer to the Sun. Examples of HDR images taken with the sky imager are given in Figure 2.



Figure 2. **Example of HDR sky images.**

At the time the work was made, the database contained more than a year of DNI and sky image data (373 days), but it is still being updated.

## 3. Reference forecasting models

In addition to the widely used smart persistence model, the proposed hybrid forecasting model is compared to two machine-learning-based algorithms using historical DNI data only, to assess the usefulness of incorporating sky images in the forecasting process.

### 3.1. Persistence model

This model is based on the simple supposition that DNI is not going to change over the considered forecast horizon  $H$ :

$$\widehat{\text{DNI}}(t + H) = \text{DNI}(t)$$

Even though it is an extremely naïve approach, the persistence model gives very good results when the forecast horizon is low. Of course, this model's performance degrades as the forecast horizon increases and when DNI presents high variability.

### 3.2. Smart persistence model

The persistence model can be improved by The DNI can be decomposed into two components:

$$\text{DNI}(t) = k_c(t) \cdot \text{DNI}_{\text{CS}}(t)$$

Where  $\text{DNI}_{\text{CS}}$  is the clear-sky DNI (the DNI value that would be obtained if the sky was clear), and  $k_c$  is the clear-sky index, that translates the attenuation due to atmospheric disturbances. The smart persistence model is based on the supposition that the clear-sky index is constant over the forecast horizon. Therefore, the DNI forecast is obtained as:

$$\begin{aligned}\widehat{\text{DNI}}(t + H) &= k_c(t) \cdot \widehat{\text{DNI}}_{\text{CS}}(t + H) \\ &= \frac{\text{DNI}(t)}{\text{DNI}_{\text{CS}}(t)} \cdot \widehat{\text{DNI}}_{\text{CS}}(t + H)\end{aligned}$$

The smart persistence model thus needs clear-sky DNI forecasts, which are provided

by a clear-sky DNI model. Many clear-sky models exist, among which the model developed in [Nou-2016a] has been chosen due to its high accuracy and adaptive nature.

### 3.3. Machine-learning-based models

#### 3.3.1. LSTM model

The first proposed model is based on a long short-term memory (LSTM) network. It consists of multiple layers of LSTM units, followed by a fully connected layers combining the output of the LSTM layers, to perform the forecast (see Figures 3 and 4). The LSTM units are used to face both the common exploding-gradient and vanishing-gradient problems, and can be divided into three main parts: the ‘forget gate’, responsible for the portion of data to be ignored; the ‘input gate’, which updates the status of the unit; finally, the ‘output gate’, that determines the current hidden state used for the computation of the unit's status during the next time step.

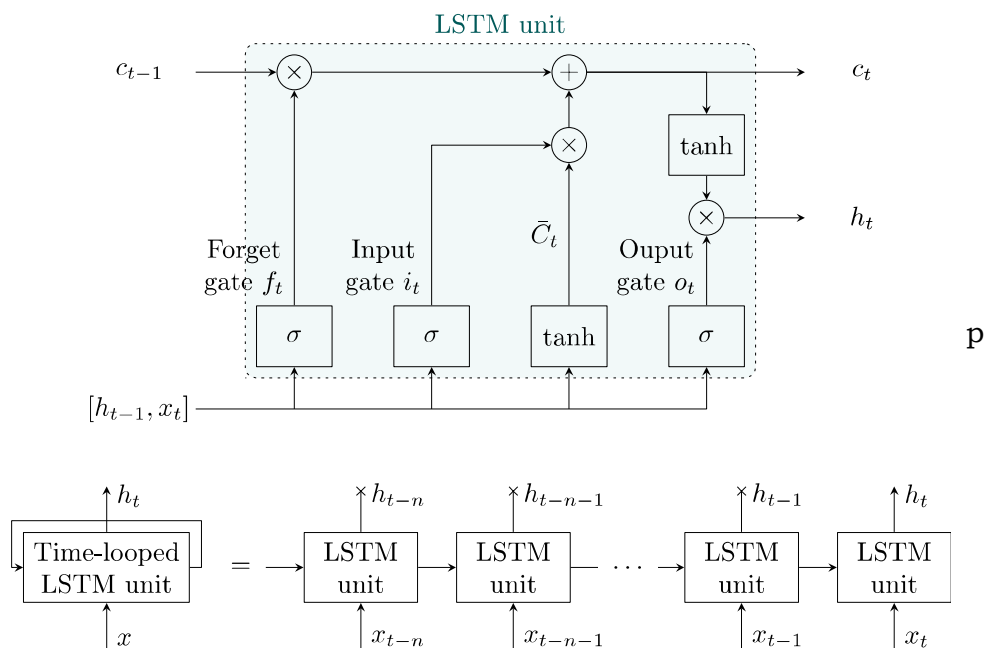


Figure 3. **Above: a LSTM unit defined by its three main gates (forget, input, and output gates). Below: an unfolded time-looped LSTM unit.**

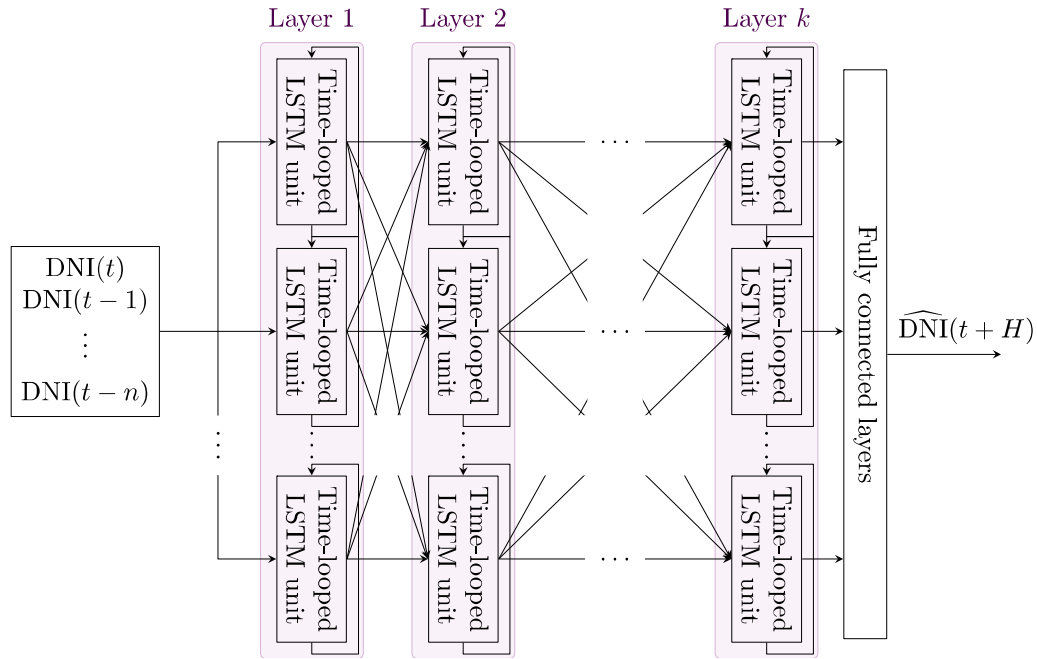


Figure 4. **LSTM model structure, with LSTM layers followed by fully connected layers, taking past DNI observations as time-support, and providing a DNI forecast at horizon H.**

### 3.3.2. CNN-LSTM model

The second proposed model is a convolutional neural network / long short-term memory (CNN-LSTM) network, consisting of a convolutional layer, serving as a preprocessing step to extract features to facilitate DNI forecasting, LSTM layers and fully connected layers (see Figure 5). This type of network is used when there is a spatial structure in the input, as in an image, or when there is a temporal structure in the input, such as a sequence of images (video) or values (time series). It can also be used when the output possesses a temporal structure, such as in multi-horizon time series forecast models.

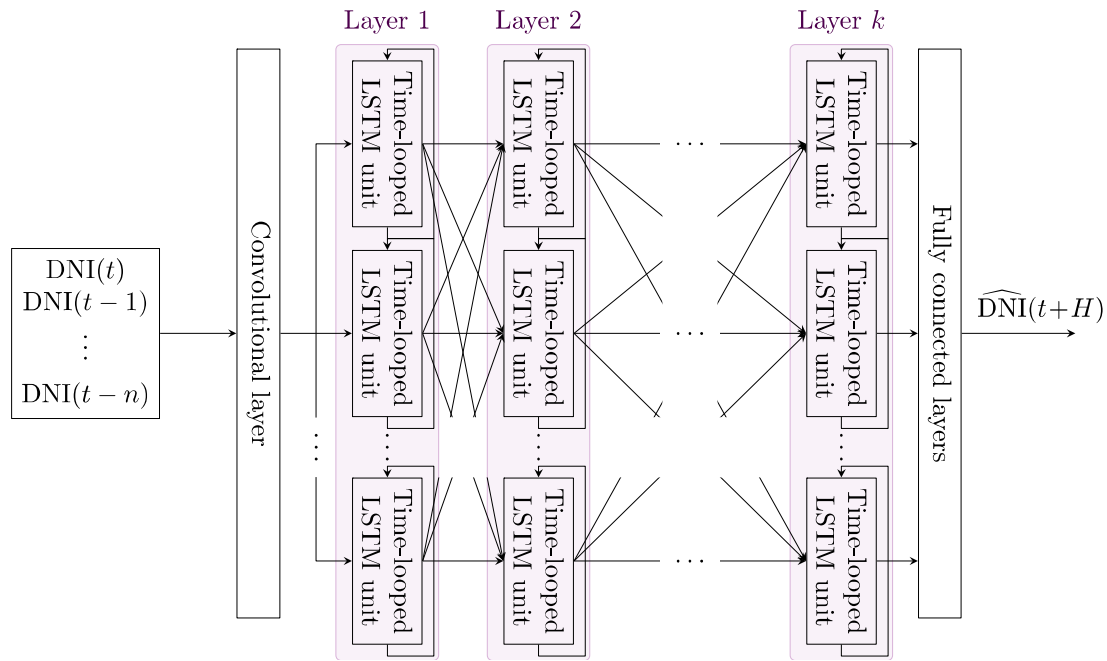


Figure 5. **CNN-LSTM model structure with a convolutional layer, LSTM layers, and fully connected layers, taking past DNI observations as time-support, and providing a DNI forecast at horizon H.**

### 3.3.3. Implementation of machine-learning-based models

Both the LSTM and the CNN-LSTM networks are trained and validated using a cross-validation technique: the training dataset is randomly but equally divided into five groups of samples called folds; in each fold 70% of data is used for training and 30% for validation. Adaptive moments (Adam), a computationally-efficient stochastic gradient descent optimization method based on an adaptive estimation of the momentum, is used. To prevent overfitting, dropout regularization is performed for each layer in the network with a rate of 50%. The loss function is chosen to be the mean squared error over the mean average error. Finally, the models are trained using 20 epochs for each fold where convergence is assured.

### 3.4. Proposed hybrid forecasting model

The proposed hybrid forecasting model uses sky images to detect clouds and determine their motion, which permits to localize a region of interest (ROI). This ROI is supposed to interact with the Sun after the considered forecast horizon. After its localization, some features are extracted from the ROI and fed to a forecast model to provide DNI forecasts. The different components of the model, that can be seen in Figure 6.

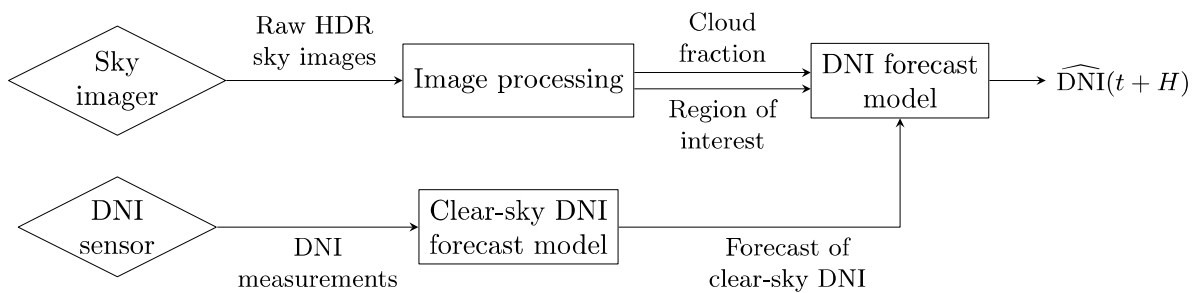


Figure 6. **Global architecture of the proposed hybrid model, showing three main parts: image processing, clear-sky DNI forecast model, and DNI forecast model.**

#### 3.4.1. Image processing

This step is crucial in the DNI forecasting process, since the sky conditions should be accurately analysed to provide accurate forecasts. Image processing is used to extract information relevant to DNI forecasts. Figure 7 summarizes all the image processing steps leading to the extraction of features from the sky images:

- the HDR images are treated to correct the fisheye lens distortion,
- a low dynamic image is generated to be used in the cloud estimation method,
- clouds are detected using a developed machine-learning-based model,
- cloud motion is then estimated using the Farnebäck optical flow algorithm,
- the cloud fraction in the ROI is calculated and fed to the DNI forecast model.

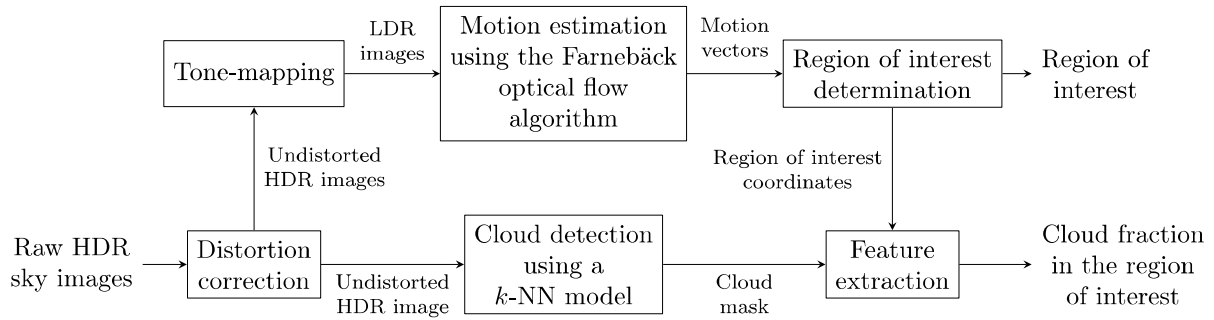


Figure 7. **Image processing steps: distortion correction, cloud detection and cloud motion estimation. The region of interest (ROI) is then located and the cloud fraction in the ROI is calculated.**

### 3.4.2. DNI forecast model

As can be seen in Figure 8, the DNI forecast model that appears in Figure 6 is divided into three main parts. The first part, responsible for image feature extraction, is a convolutional neural network (CNN). The second part is a multi-layer perceptron (MLP) with the cloud fraction in the region of interest and the clear-sky DNI forecast as inputs. The outputs of the CNN and the MLP networks are then fed to a ‘Regression MLP’, used to merge extracted features and provide the DNI forecast.

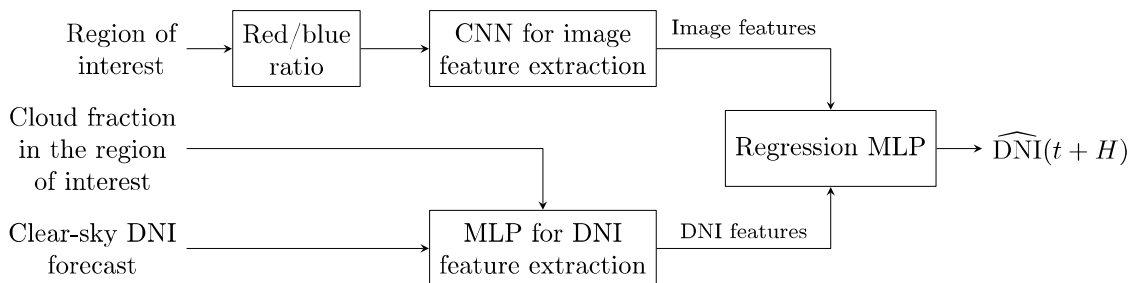


Figure 8. **The three main parts of the DNI forecast model.**

The database used to train the neural networks consists of 40 days, each with 1200 observations (sky images and DNI measurements) starting from 7:00 AM till 5:00 PM, with 30 seconds sampling time. This database is split into 22 days for training and cross-validation (representing 26400 observations), 16 days for testing (representing 19200 observations), and two days for cases studies (representing 2400 observations). The DNI forecast model is trained and validated using a cross-validation technique: the dataset is randomly but equally divided into five groups of samples called folds; in each fold 70% of data is used for training and 30% for

validation. Adaptive moments (Adam), a computationally efficient stochastic gradient descent optimization method based on an adaptive estimation of the momentum, is used. To prevent overfitting, dropout regularization is performed for each layer in the network with a rate of 50%. After testing, the loss function is chosen to be the mean squared error over the mean average error. Finally, the models are trained using 20 epochs for each fold in order to assure convergence.

## 3.5. Forecasting results

### 3.5.1. Performance metrics

- The root mean squared error (RMSE) is calculated as follows:

$$\text{RMSE} = \sqrt{\frac{1}{n} \sum_{t=1}^n \left( \text{DNI}(t) - \widehat{\text{DNI}}(t) \right)^2}$$

- The normalized root mean squared error (nRMSE) is calculated as follows:

$$\text{nRMSE} = \frac{\sqrt{\frac{1}{n} \sum_{t=1}^n \left( \text{DNI}(t) - \widehat{\text{DNI}}(t) \right)^2}}{\frac{1}{n} \sum_{t=1}^n \text{DNI}(t)}$$

- The skill factor (SF) is employed to evaluate the models' performance versus the smart persistence model; it is defined as:

$$\text{SF} = 100 \cdot \left( 1 - \frac{\text{nRMSE}_M}{\text{nRMSE}_{PE}} \right)$$

where  $\text{nRMSE}_M$  and  $\text{nRMSE}_{PE}$  are the nRMSE of the proposed model and the smart persistence model, respectively.

- The mean average error (MAE) is calculated as follows:

$$\text{MAE} = \frac{1}{n} \sum_{t=1}^n \left( \text{DNI}(t) - \widehat{\text{DNI}}(t) \right)$$

- Finally, a metric called the ramp detection index (RDI) is used. It is designed to evaluate the ability of the model to predict ramps, which have an important impact on CSP plants: predicting them can thus be helpful in the control process. First, the ramp magnitude (RM) is calculated as:

$$RM(t) = \frac{|DNI(t) - DNI(t + H)|}{\widehat{DNI}_{CS}(t)}$$

Usually, high-magnitude ramps are defined by  $RM > 0.5$  and moderate ramps by  $0.3 < RM < 0.5$ . A ramp detection (also called a *hit*) is achieved if both the following conditions are satisfied:

$$RM(t) > 0.15$$

$$\text{sign}(DNI(t) - \widehat{DNI}(t + H)) = \text{sign}(DNI(t) - DNI(t + H))$$

The ramp is not detected (a *miss*) if the first equation above is met while the second is not. Finally, the RDI is calculated as:

$$RDI = \frac{N_{hit}}{N_{hit} + N_{miss}}$$

where  $N_{hit}$  and  $N_{miss}$  are the numbers of hits and misses, respectively.

### 3.5.2. Comparison of forecasting results

In this section, the hybrid model is compared to the reference models: smart persistence and machine-learning-based models using past DNI observation only. First, the models' performance on clear-sky, overcast, and mixed situations are compared. Then, two cases with different DNI variability are studied to gain more insight on the accuracy and performance of the hybrid model.

#### 3.5.2.1. Global comparison

The forecasting results, in case of mixed situations, can be found in Figure 9: the hybrid model scores the lowest nRMSE values and the highest SF and RDI for each forecast horizon. LSTM and CNN-LSTM models, which are based on past DNI observations only, do not forecast DNI ramps as well as the hybrid model: cloud motion is indeed critical to better anticipate DNI variations. This superior performance justifies the integration and processing of HDR sky images, that

translates into better ramp detection and accurate DNI forecasts compared to the models based on DNI measurements only. Finally, the CNN-LSTM slightly outperforms the LSTM model thanks to its additional convolutional layer.

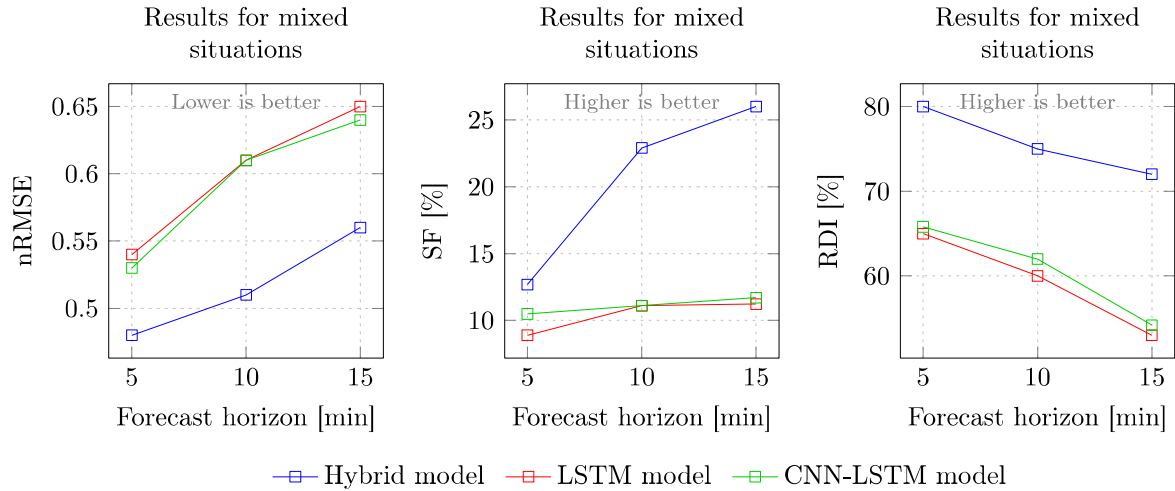


Figure 9. **Comparison between LSTM, CNN-LSTM, and hybrid models on mixed situations.**

The results of the comparison on clear-sky days and overcast days from different seasons is given in Figure 10. The smart persistence model generally scores very low nRMSE values on such cases. As already seen in Figure 9, the hybrid model consistently outperforms the smart persistence model for each forecast horizon, with a SF ranging between 6% and 9.5%. The low nRMSE values and the positive SF scored by the hybrid model confirm that the model learned to distinguish clear-sky and completely overcast situations. However, on such low-variability situations, the results obtained by the LSTM and CNN-LSTM models are considerably inferior to the results obtained by the smart persistence model. Contrary to the hybrid model, they are not able to correctly handle these situations: although the nRMSE they obtain is low, the smart persistence model is so performant in these cases that the RNN models score negative SF values (around -120% for H=5 min, -50% for H=10 min and -25% for H=15 min). This demonstrates the benefits of including sky images in the forecasting process.

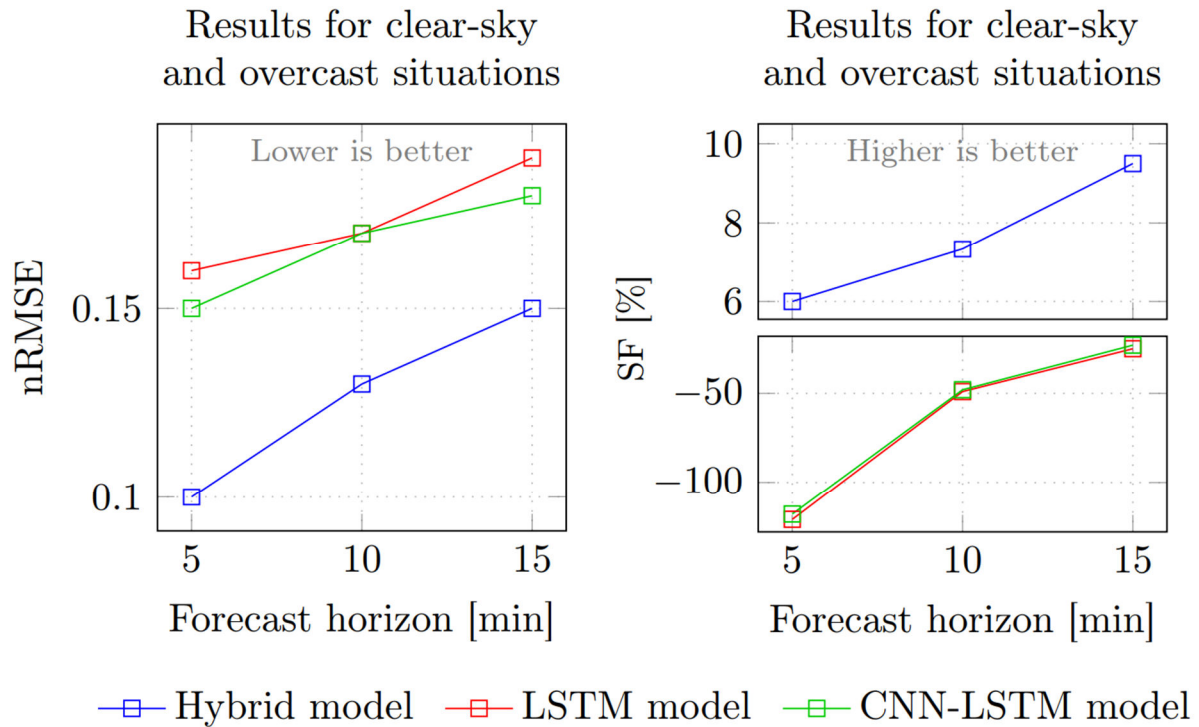


Figure 10. **Comparison between LSTM, CNN-LSTM, and hybrid models on clear-sky and overcast situations.**

### 3.5.2.2. Case studies

A low-variability case is presented in Figure 11: most of the day features a clear-sky situation, with thin clouds in the morning and the evening. The smart persistence model typically provides great results on such days: here, it outperforms both the LSTM and CNN-LSTM models, but the hybrid model still manages to come up with better results.

Thin clouds pose some serious problems for ordinary methods based on the cloud fraction, since they usually do not take into consideration clouds' thickness, leading to overestimation of the cloud fraction. As shown in Figure 11 before 10:00 and after 16:00, the hybrid model is able to correctly handle these cases.

Let us focus now on a specific instant during the day: in Figure 11, the sky image taken at 15:30 is presented -- precisely 15 min before a drop in DNI. The forecast given by the hybrid model shows a decrease in DNI because of the presence of clouds in the ROI, and, as predicted, a negative ramp takes place 15 min later.

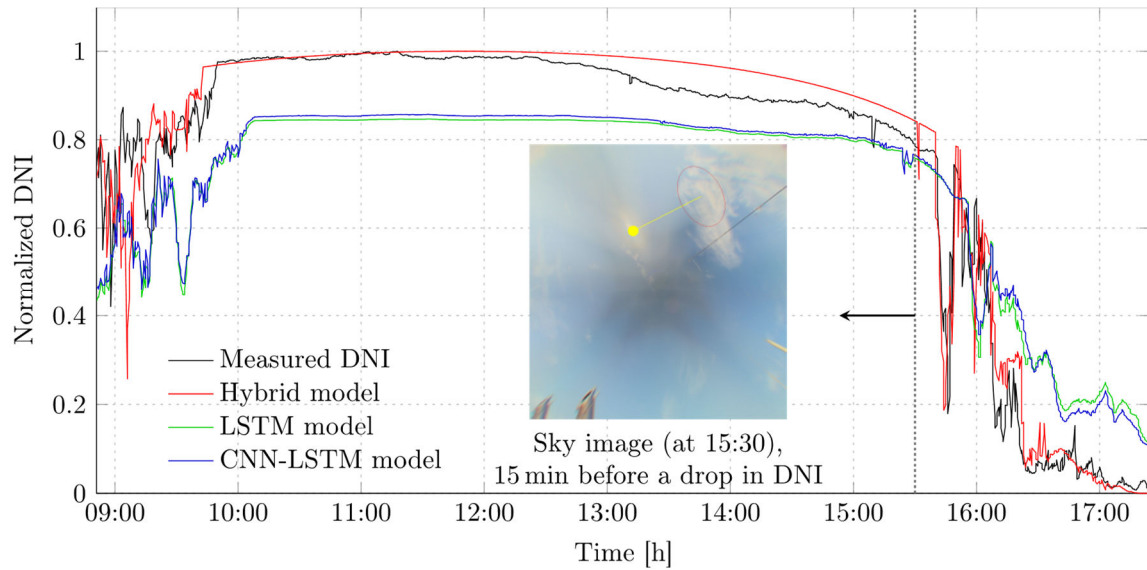


Figure 11. **Low-variability DNI forecast at horizon  $H=15$  min.**

A high-variability day is now presented in Figure 12. After a few hours of clear-sky (until 10:00), sudden high-frequency variations are observed. This case is challenging due to these fast and hard-to-predict DNI variations. Here, the smart persistence model performs very poorly, and, while better, the LSTM and CNN-LTM models do not give satisfactory results either; again, the hybrid model performs significantly better.

This high-variability day is a good example of the HDR sky images' contribution in the forecasting process: the LSTM and CNN-LSTM models are not able to predict DNI ramps, while the hybrid model is able to anticipate them due to the cloud motion analysis. In particular, the hybrid model is able to predict sudden DNI variations in the period between 11:00 and 13:00. The LSTM and CNN-LSTM models, however, fail to predict most of the ramps and perform poorly.

Let us focus now on two specific instants during the day.

- Sky image 1, taken at 10:52, shows a situation with clouds in the ROI, leading to the correct forecast of a negative ramp 15 min later. Note also that the clouds are not in the center of the ROI: had a ROI of the same size as the Sun been chosen, that negative ramp would not have been correctly forecast.
- Sky images 2 and 3, taken at 15:25 and 15:40, respectively, feature a complicated sky situation, with thin clouds around the Sun and thick clouds approaching. In this situation, methods without special treatment for thin

clouds would perform poorly. The proposed hybrid model proves to be robust and manages to detect the ramp provoked by the thick clouds that are in the ROI in sky image 2 and are starting to block the Sun 15 min later.

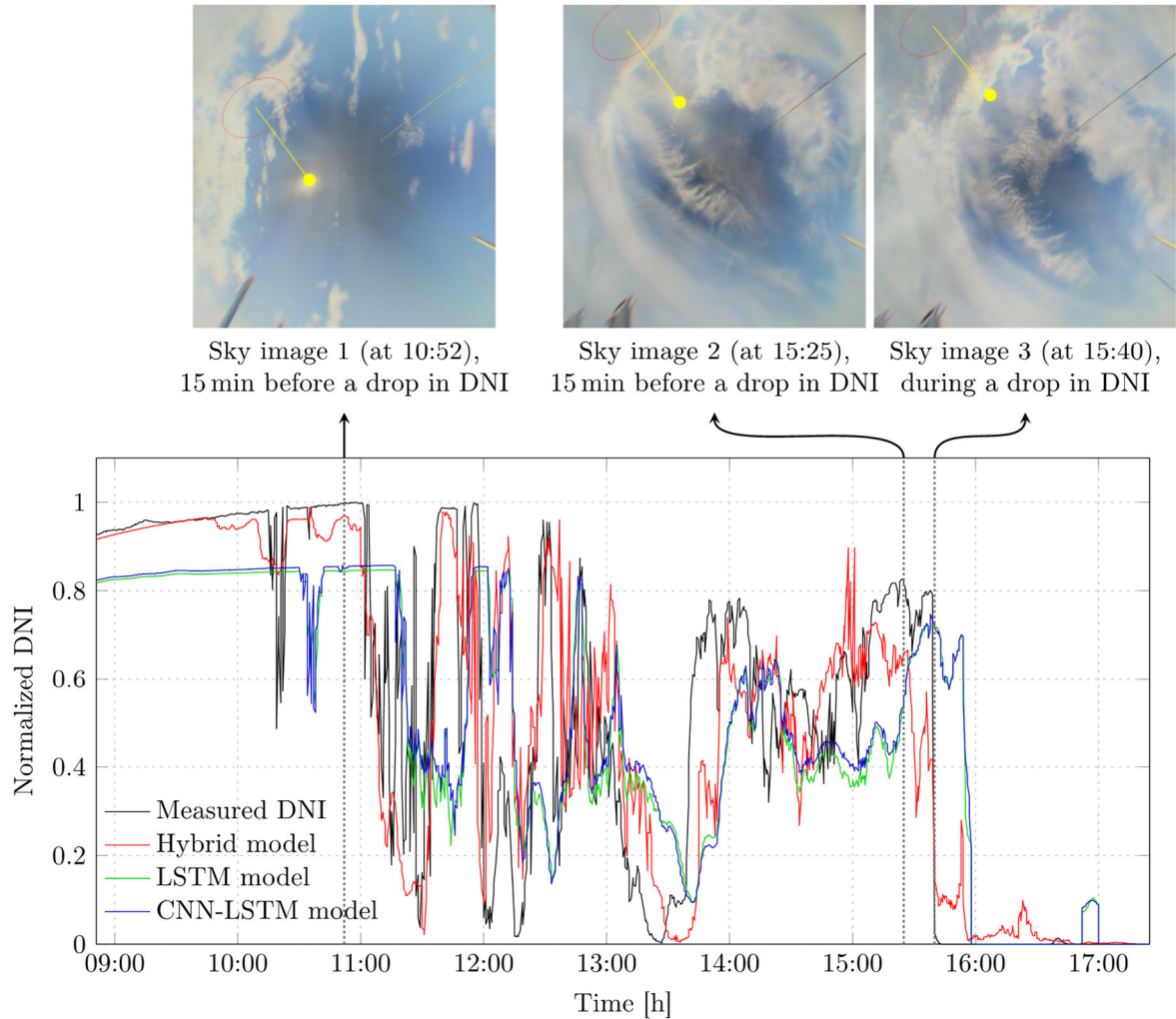


Figure 11. **High-variability DNI forecast at horizon H=15 min.**

## 3.6. Online implementation of the hybrid model

The goal of the development of the hybrid model is to provide accurate DNI forecasts in real time. This model has thus been implemented on a server. The HDR sky images are transferred every 30 seconds to a hard drive, and the algorithm is able to read the HDR sky images stream and perform all the image processing tasks in real time to provide DNI forecasts. For every time step and after the code execution, the code registers in a Json file including the DNI forecasts, a description of the sky situation (clear-sky, overcast, or mixed) derived from the cloud segmentation model, and the cloud motion estimation (magnitude and direction). Finally, a sky image with the ROI is saved to help understand the provided forecasts. This information is provided to CSP infrastructure users via a graphical user interface (GUI), as shown in Figures 12 and 13.



Figure 12. **The GUI providing DNI forecasts to RI users in Odeillo, France.**



Figure 13. **The GUI providing DNI forecasts to RI users in Odeillo, France.**

## 3.7. Conclusion

A hybrid intrahour forecast model has been developed, combining knowledge-based and machine-learning approaches and taking DNI measurements and HDR sky images as inputs. This hybrid model is compared to LSTM and CNN-LSTM models that take only past DNI observations as input, to assess the benefits of integrating HDR sky images in the forecasting process. The smart persistence model is also used as reference for the comparison.

Various image processing steps are performed in the proposed hybrid model. Cloud segmentation and cloud motion estimation allow to determine an adaptive region of interest. The forecasting step is performed using a combination of two neural networks: a CNN, which processes the region of interest, and a MLP that takes the cloud fraction in the region of interest and a forecast of the clear-sky DNI as inputs to finally forecast DNI at horizons between 5 min and 15 min.

For mixed situations, results show that while all the tested machine-learning-based models are capable of outperforming the smart persistence model, the hybrid model is clearly ahead. The ramp detection index shows that the hybrid model is able to forecast 72% to 80% of the ramps, whereas the LSTM and CNN-LSTM models are less efficient and detected between 53% and 66% of the ramps. This difference is due to the fact that LSTM and CNN-LSTM models are purely statistical and rely solely on past DNI observations to perform forecasts, without taking into account the sky situation: efficient cloud detection and accurate cloud motion estimation translates into better ramp detection and accurate DNI forecasts.

For clear-sky and overcast situations, the smart persistence model produces very good results, and the results obtained by the LSTM and CNN-LSTM models are considerably inferior. However, the hybrid model still manages to outperform the smart persistence model, with skill factor values ranging from 6% to 9.5%. Thanks to the inclusion of HDR sky images, it successfully manages clear-sky, overcast, and mixed situations. As for the complexity of the models, the analysis shows that, while the hybrid model is more complex, time-consuming, and demands more computational resources, it is still able to provide forecasts within 7% of the 30s sampling time.

Finally, the proposed model has been implemented in situ to provide real-time DNI forecasts to RI users.

## List of abbreviations

---

DNI	Direct normal irradiance
CNN	Convolutional neural network
MLP	Multi-layer perceptron
LSTM	Long short-term memory
RMSE	Root means square error
nRMSE	Normalized root mean square error
MAE	Mean average error
SF	Skill factor
RDI	Ramp detection index
ROI	Region of interest
HDR	High dynamic range
NWP	Numerical weather prediction
RM	Ramp magnitude

## Annexes

In case additional details on the developed algorithms are needed, we provide in the sequel two additional documents:

1. A scientific article published in the journal “Solar Energy”:

*Y. Karout, S. Thil, J. Eynard, E. Guillot, and S. Grieu. Hybrid intrahour DNI forecast model based on DNI measurements and sky-imaging data. Solar Energy, 249:541–558, Jan. 2023.*

It focuses on the proposed hybrid DNI forecast model, using sky images and DNI measurements to provide forecasts at 5 min, 10 min and 15 min.

2. The PhD thesis written by Youssef KAROUT:

*Y. Karout. Pr evision de l’ claircissement normal direct par intelligence artificielle et commande pr dictive d’un r acteur solaire. PhD thesis, Universit  de Perpignan Via Domitia, Dec. 2022.*

It is written in English, with an extended abstract in French. It provides more details on the developed approach, and also additional work on the model-based predictive control of a solar reactor dedicated to syngas production (task 8.3 of WP8), for which an another DNI forecast model has been developed, inspired by the previous one, but adapted to lower forecast horizons (0.5 min to 2.5 min).

## **Annex 1. References**

[Nou-2016a] J. Nou, R. Chauvin, S. Thil, and S. Grieu, “A new approach to the real-time assessment of the clear-sky direct normal irradiance,” Applied Mathematical Modelling, vol. 40, pp. 7245–7264, Aug. 2016.

## **Annex 2. Scientific article published in “Solar Energy”**

DOI: <https://doi.org/10.1016/j.solener.2022.11.032>

Link (3 MB): <https://mycore.core-cloud.net/index.php/s/gIkqTSXupGiXSjt>

## **Annex 3. Complete PhD thesis**

Link (48 MB): <https://mycore.core-cloud.net/index.php/s/YlpC9jDoBIGmp47>